Cite this article as:

Marcos, J.V. and Cristóbal, G., 2013. Texture classification using discrete Tchebichef moments. Journal of the Optical Society of America A, 30(8), pp.1580-1591.

DOI: https://doi.org/10.1364/JOSAA.30.001580

Texture classification using discrete Tchebichef moments

J. Víctor Marcos[1,*] and Gabriel Cristóbal[1]

[1]Instituto de Óptica (CSIC), Serrano 121, 28006 Madrid, Spain

**Corresponding author: jvmarcos@gmail.com*

In this paper, an innovative method to characterize texture images based on discrete Tchebichef moments (DTM) is presented. A global signature pattern is derived from the moment matrix by taking into account both the magnitude of the moments and their order. The performance of our method for several texture classification problems was compared with that achieved through other standard approaches. These include Haralick's gray level co-occurrence matrices (GLCM), Gabor filters (GF) and local binary patterns (LBP). An extensive texture classification study was carried out by selecting images with different contents from Brodatz, Outex and VisTex databases. The results show that the proposed method is able to capture the essential information about texture showing comparable or even higher performance than conventional procedures. Thus, it can be considered as an effective and competitive technique for texture characterization.

OCIS codes: 100.2000, 100.5010, 150.1135

1. Introduction

Texture has been a subject of study for the image processing community during the last decades. However, there is no consensus about its definition. Tuceryan and Jain [1] compiled the definitions provided by different researchers. According to them, texture is a property related to the roughness of a surface and is characterized by the variation of pixel intensity in the spatial domain. Texture can be found in images of different nature. For instance, a specific body tissue, an area of terrain, the surface of an object or the skin of a person or an animal. Thus, an accurate characterization of texture properties is required in different real-world applications involving image processing. Specifically, texture plays a relevant role in tasks such as medical diagnosis [2], remote sensing [3] or biometric identification [4].

Mainly, texture analysis deals with four types of tasks: texture classification, texture edge identification, texture synthesis and the shape-from-texture problem [1]. The former is addressed in the present study. Texture classification aims to automatically identify image regions characterized by different texture properties. Thus, the attributes that differentiate each texture from the other ones must be captured. Several methods have been proposed in the literature to perform texture classification. They are conventionally grouped into four categories [1]: (i) statistical methods, (ii) geometrical (structural) approaches, (iii) model-based techniques and (iv) signal processing methods based on spatial and frequency domain filtering. Signal processing-based methods represent a traditional approach to texture characterization [5]. Experimental results suggest that the human brain identifies textures by means of space-frequency analysis of the input image [6]. As a result, this behaviour has been simulated through signal processing techniques based on image filtering. Indeed, a number of studies focused on texture classification propose frequency-based and spatial frequency-based analysis of the image. For instance, filter

banks [7], wavelets [8] and Gabor filters [9, 10] have proven to be a valid technique for automatic texture identification, showing high classification performance.

Closely related to signal processing techniques, image moments have been widely used for pattern recognition tasks and they suitably adapt to texture analysis [12]. It is worth noting the pioneering work on the construction of moment invariants performed by Hu [11] in the 60's. Moments are scalar quantities used to characterize a function (image), reflecting significant attributes of it. Mathematically, the moment T_{pq} of an image $f(x, y)$, where p and q are non-negative integers and $s = p + q$ denotes its order, is computed from the projection of the image onto a polynomial basis $r_{pq}(x, y)$ defined on a region D: $T_{pq} = \iint_D r_{pq}(x,y) f(x,y)\, dxdy$ [12]. Thus, the value of T_{pq} measures the correlation between the image $f(x, y)$ and the corresponding polynomial function $r_{pq}(x, y)$. Several moment families have been defined in the literature by using different polynomial basis. They can be grouped as non-orthogonal and orthogonal depending on the behaviour of the basis functions. The former group include geometric and complex moments, which represent a conventional approach for image analysis [11]. Indeed, these moments were previously used for feature extraction from texture images [13, 14]. However, as the basis set used to compute geometric and complex moments is non-orthogonal, a redundant representation of the information contained in the image is obtained [15]. Additionally, non-orthogonality causes the problem of image recovery from these moments to be strongly ill-posed and computationally expensive [16]. Continuous orthogonal moments such as Legendre and Zernike families were introduced to overcome these drawbacks [2, 17, 18]. Nevertheless, practical implementations of continuous moments lead to two main sources of error. First, their exact definition involves the calculation of integrals that are approximated by summations in the discrete domain. Second, Legendre and Zernike polynomials are defined in a

specific region of the space. It is given by the interval between -1 and 1 for Legendre polynomials while Zernike functions are defined in the unit circle. Thus, the image coordinate space must be transformed for their computation [15, 19].

Discrete orthogonal moments avoid these limitations and hold most of useful properties of continuous orthogonal moments. This is achieved by defining a set of orthogonal polynomials in the image space. As a result, the discretization error inherent to continuous moments is prevented while enabling accurate image reconstruction [19]. Commonly, discrete Tchebichef [15] and Krawtchouk [20] polynomials are used to compute discrete orthogonal moments. For a digital image $f(x, y)$ with $0 \leq x, y \leq N - 1$, a total of N^2 moments can be extracted. The entire moment set is required for a complete description of the image, i.e., to ensure perfect image reconstruction. Nevertheless, computation of high order moments is affected by numerical instabilities motivated by the recurrence equations used to obtain polynomial coefficients [12]. As a result, numerical errors are propagated and accumulated with increasing moment order and image size [19]. To avoid this problem, Mukundan et al. [21] defined scaled Tchebichef polynomials. They are obtained by normalizing Tchebichef polynomials by a factor that depends on their order. The computational approach suggested by Mukundan allows the complete set of discrete Tchebichef moments (DTM) characterizing an image to be computed.

In this study, a novel method based on DTM is proposed to characterize digitized texture images. DTM can yield relevant texture features since they represent the outputs from different band-pass filters given by the Tchebichef kernels [22]. The oscillating shape of these functions reflects the correspondence between frequency and moment order, with higher frequency components being linked to higher order moments [22, 23]. In our method, only the magnitude of the moments was considered to perform texture feature extraction. It provides information

about the similarity of the input image and the polynomial kernel. Hence, higher magnitude is expected for those moments derived from kernel functions showing fluctuating patterns similar to the texture. In agreement with the correspondence between frequency and moment order, a signature pattern $M(s)$ is obtained from the texture image by assessing the total moment magnitude for a given order s. This pattern $M(s)$ reflects the global response of the texture to the set of kernel functions with the same order. A similar strategy was adopted by Yap et al. [23] to develop a focus measure based on DTM as the energy ratio between moments of high order and moments of low order. For the proposed texture classification task, two desirable results are derived from this order-based grouping approach. First, the dependence of the proposed feature pattern on the moment order enables the interpretation of texture properties. For instance, a higher value of $M(s)$ at order s indicates that texture contains patterns of variation that occur at the frequencies represented by the kernel functions of that order. As shown in the present study, the plot of $M(s)$ versus s can be used for a qualitative evaluation of the texture. Second, a notable reduction of dimensionality is obtained. For a N x N image, the initial moment set composed of N^2 coefficients is mapped onto a pattern of dimension $2N - 1$. The curse of dimensionality must be taken into account when modelling multivariate data since it may lead to undesired overfitting effects [24]. Thus, low dimensionality enables pattern analysis techniques to be used in an efficient manner.

Previously, DTM have been applied to problems such as image quality assessment [22, 25], digital watermarking [26], image autofocus [23], detection of image modifications [27] or image compression [28]. To our knowledge, only a reduced number of studies have been focused on the use of DTM to describe texture features. These were basically devoted to texture analysis in medical applications. In particular, low order DTM were suggested to characterize colour

texture features in gastrointestinal tract images from endoscopy [29]. In a different vein, a combination of several moment families, including DTM, was proposed to represent texture regions in CT liver images [30]. Moments up to order four were considered for regions of size 21 x 21 pixels. On the other hand, discrete cosine transform (DCT) coefficients, which are computed from a polynomial basis similar to that of DTM [31], have been used for texture characterization [32]. DCT-based analysis was conceived as an effective approach for processing JPEG compressed images. For this purpose, image processing is carried out on 8 x 8 blocks as defined by the standard [32].

The aim of this study is to assess the utility of the proposed DTM-based method for automatic identification of texture images. A supervised pattern classification approach is used to model this task. Thus, given a texture image, the goal is to determine to which category it belongs among a finite number of possible choices. Regularized discriminant analysis (RDA) [33] is proposed to implement the pattern classification stage. Texture images from several public databases including Brodatz [34], Outex [35] and VisTex [36] have been used to validate our methodology. An exhaustive evaluation of the method is presented, analyzing the influence of the image size and rotation on classification performance. For a fair validation, several well-known techniques for texture analysis such as Haralick's gray level co-occurrence matrices (GLCM) [37], Gabor filters (GF) [38] and local binary patterns (LBP) [39] were used as a reference. A comparative analysis of the results achieved by these methods and the approach presented in this study is provided.

The paper is organized as follows. The second section includes a detailed description of the method presented in this study. A brief introduction to the methods selected for comparison purposes is also included. The third section details the image datasets used to validate our

method as well as the experiments carried out. The results achieved by our method and the reference techniques are presented. Finally, a discussion of our results and a summary of the main findings of our study are included in the fourth section of the paper.

2. Methods

Texture classification involves two main tasks: feature extraction and classification [37]. The former maps the texture image onto a set of descriptors or features. These are expected to provide valuable information about the texture in order to be assigned to the correct category among several possibilities. The feature set constitutes a pattern vector that summarizes the information in the image. This pattern is fed into a classifier, which performs the second task in the texture classification process. The selection of the classifier is usually motivated by the number of available samples and the dimension of the feature pattern [24].

The present study is focused on the feature extraction stage. A novel feature pattern is proposed to represent texture properties. In order to assess its utility, it was compared with other methods that have been proven to be effective in texture feature extraction: GLCM, GF and LBP. For a fair comparison, the same classification approach was used to process the features derived from each of these methods. RDA developed by Friedman [33] was selected for this purpose since it suitably adapts to both high and low dimensional feature patterns. The four texture feature extraction methods and the RDA classifier are presented in this section.

2.1. Discrete Tchebichef moments

Discrete Tchebichef moments (DTM) were introduced by Mukundan et al. [15] in order to overcome the limitations of conventional orthogonal moments based on Legendre and Zernike polynomials. DTM are computed by projecting the original image $f(x, y)$ ($x, y = 0, 1, \ldots, N - 1$)

onto a set of Tchebichef polynomial kernels, which include basis functions of the DCT as a special case [31]. The moment T_{pq} (p, q = 0, 1, …, N - 1) of order $r = p + q$ is defined as [15]:

$$T_{pq} = \frac{1}{\tilde{\rho}(p,N)\tilde{\rho}(q,N)} \sum_{x=0}^{N-1} \sum_{y=0}^{N-1} \tilde{t}_p(x) \tilde{t}_q(y) f(x,y), \tag{1}$$

where $\tilde{t}_n(x,N)$ is the scaled Tchebichef polynomial of degree n and $\tilde{\rho}(n,N)$ is its squared norm. The polynomial $\tilde{t}_n(x,N)$ is a modified version of the discrete Tchebichef polynomial $t_n(x,N)$ by including a scale factor $\beta(n,N)$:

$$\tilde{t}_n(x,N) = t_n(x,N) / \beta(n,N). \tag{2}$$

Mukundan et al. [21] proposed a computational procedure to ensure numerical stability of DTM even in the case of large values of the polynomial degree n and/or the image dimension N x N. It requires using the following value for the scale factor:

$$\beta(n,N) = \left[\frac{N\left(N^2-1\right)\left(N^2-2^2\right)\cdots\left(N^2-n^2\right)}{2n+1} \right]^{1/2}, \tag{3}$$

which results in an orthonormal basis of scaled Tchebichef polynomials $\tilde{t}_n(x,N)$, i.e., $\tilde{\rho}(n,N) = 1$. The orthogonality property of the obtained basis ensures exact image reconstruction from the set of moments T_{pq}:

$$f(x,y) = \sum_{p=0}^{N-1} \sum_{q=0}^{N-1} T_{pq} \tilde{t}_p(x) \tilde{t}_q(y). \tag{4}$$

According to (1), the value of T_{pq} can be interpreted as the correlation between the image $f(x, y)$ and the kernel function $r_{pq}(x, y)$ built from discrete Tchebichef polynomials, which is given by:

$$r_{pq}(x,y) = \frac{1}{\tilde{\rho}(p,N)\tilde{\rho}(q,N)} \tilde{t}_p(x)\tilde{t}_q(y). \quad (5)$$

These kernel functions are characterized by an oscillating behaviour, showing a sine-like profile. Figure 1 shows the Tchebichef kernels for $N = 8$. In the spatial domain, the kernel function oscillates along both x and y coordinates. Additionally, the fluctuation rate in a given direction increases with the order of the corresponding polynomial. It shows that higher frequency components are related to kernels derived from polynomials of higher order [22].

INSERT FIGURE 1 AROUND HERE

The kernel $r_{pq}(x, y)$ can then be viewed as a filter for the computation of T_{pq}. Indeed, it is worth noting that T_{pq} is obtained from sampling the input image by means of $r_{pq}(x, y)$ [22]. Therefore, the magnitude of T_{pq} will be higher for images oscillating at a similar rate to $r_{pq}(x, y)$ along both directions. This is an interesting property for texture analysis since texture involves the spatial repetition of intensity patterns [1]. Thus, the magnitude of DTM can yield relevant information about texture. A description of texture properties can be obtained by assessing the dependence of the moment magnitude on the order s, which reflects the frequency content of the kernels. For this purpose, the following feature pattern $M(s)$ ($s = 0, 1, \ldots, 2N - 2$) is proposed:

$$M(s) = \sum_{p+q=s} \left| T_{pq} \right|. \quad (6)$$

The value of $M(s)$ quantifies the global response to the set of kernel functions determined by s. Qualitatively, $M(s)$ can be interpreted as a similarity measure between the image $f(x, y)$ and kernels of order s. Higher values of $M(s)$ are obtained if $f(x, y)$ contains fluctuating patterns that occur at the rate of variation of the kernels with the specified order. According to the relationship between frequency and moment order, different spectral components will be associated with each element of $M(s)$. It is worth noting that the element $M(0)$ is given by the average gray value of the image. Thus, uniform changes in the illumination of the image will only affect the value of this element. On the other hand, the number of moments involved in the computation of $M(s)$ depends on s. A smaller number of moments contribute to the corresponding element of $M(s)$ as the order s is greater or less than $N - 1$.

A plot of $M(s)$ versus the order s can be considered as a texture signature. Figure 2 shows three textures ("bark0006", "food0001" and "sand0000") of size 128 x 128 pixels from the VisTex database [36] and their corresponding $M(s)$ curve. A different $M(s)$ profile is observed for them. For "bark0006", small values of $M(s)$ are observed along s when compared to the other examples, reflecting a more reduced dynamical range of the gray level. Furthermore, the most relevant components of $M(s)$, in addition to $M(0)$, are obtained for s between 3 and 9. This behaviour indicates that the texture is characterized by smooth fluctuations of intensity, resulting in higher similarity with kernels of small order. In contrast, "food0001" is distinguished by a marked peak in the $M(s)$ curve at $s = 15$. It demonstrates high correlation between the image and the kernel functions of that order. Thus, the rate of variation characterizing these kernels predominates in the texture. The third example, "sand0000", depicts an intermediate result. In this case, the value of $M(s)$ is mostly uniform, i.e., there are no peaks in the profile of $M(s)$. This

uniformity reflects a comparable similarity with kernels of different orders. Thus, the power spectrum of the image will not be concentrated on specific frequency bands.

INSERT FIGURE 2 AROUND HERE

2.2. Haralick's gray level co-occurrence matrices

Gray-level co-occurrence matrices (GLCM) were proposed by Haralick [37] as a straightforward procedure for describing texture. It is based on the assumption that the texture information is contained in the spatial relationship between gray levels. For the computation of GLCM, suppose that each of the pixels in the image is assigned one of N_g gray levels. The value of P_{ij} represents the number of occurrences of two pixels separated by a distance d in the direction determined by the angle θ, one with gray level i and the other with j ($i, j = 1, \ldots, N_g$). The GLCM matrix is composed of the set of P_{ij} values by assessing all the possible combinations between intensities i and j [37]. Note that $P_{ij} = P_{ji}$, i.e., the occurrence of (j, i) is considered as a match when computing P_{ij}, and vice versa.

The resulting matrix is a function of both the distance and the angular direction between pixels. Therefore, different matrices are obtained by varying these parameters. Usually, the elements of the co-occurrence matrix are normalized in order to represent probabilities, providing the relative frequency of occurrence for a pair of gray levels. The element $p(i, j)$ denotes the probability of finding the pair of levels (i, j) in the image, which is obtained as:

$$p(i,j) = P_{ij}\left(\sum_{i=1}^{N_g}\sum_{j=1}^{N_g} P_{ij}\right)^{-1}. \quad (7)$$

These matrices of probabilities can be used to obtain statistical features for characterizing the texture [37]. In this study, the subset of 10 features suggested in [3] was chosen to capture texture properties: energy, contrast, correlation, homogeneity, entropy, autocorrelation, dissimilarity, cluster shade, cluster prominence and maximum probability.

Parameters N_g, d and θ must be defined by the user to compute GLCM. In our study, N_g was set to 8 since this quantization level has been applied in preceding works focused on texture analysis [5]. For the displacement vector given by d and θ, the distance parameter was set to 1 while four different angle values were assessed: 0, 45, 90 and 135 degrees [3]. Thus, a total of 40 descriptors (10 statistical features for each of the four orientations) were obtained for each texture.

2.3. Gabor filters

Gabor filters (GF) were proposed by Daugman [40] to model the response of visual cortical cells. Previous experiments suggest that an image is decomposed into a number of filtered versions of it in the early stages of the human visual system. Different frequency bands and orientations were observed in each of the resulting images [9]. GF implement this processing capability by defining a set of filters in the two-dimensional frequency domain. Each of them is characterized by its central frequency in the band pass and its orientation. By choosing the number of filters in the bank, a multi-channel image processing approach is obtained. It enables multi-resolution analysis of texture images in order to capture patterns of variation occurring at different rate and orientation. Texture can be characterized by evaluating simple statistics on the filtered images [9].

A Gabor filter is expressed as a sinusoidal wave modulated by a Gaussian envelope. In the frequency domain, the filter response consists in a real-valued function characterized by a lobe around the central frequency *F*. It is given by the following equation [38]:

$$H(u,v) = \exp\left\{-\frac{\pi^2}{F^2}\left[\gamma^2\left(u'-F\right)^2 + \eta^2 v'^2\right]\right\}, \tag{8}$$

where $u' = u\cos\varphi + v\sin\varphi$, $v' = -u\sin\varphi + v\cos\varphi$, φ is the angle between the direction of the sinusoidal wave and the *x*-axis and parameters γ and η are the standard deviation of the Gaussian in the direction of the sinusoidal wave and its orthogonal direction, respectively.

These parameters determine the width of the filter in both directions. The design of the filter bank requires finding appropriate values for them. Bianconi et al. [38] conducted a study to determine the influence of these parameters on texture classification performance. They concluded that classification accuracy strongly depends on smoothing parameters γ and η whereas the number of frequencies and orientations are not crucial. In our experiments, the filter was designed according to the considerations reported in that study. Hence, 4 different central frequencies, 6 orientations, a maximum central frequency of 0.327 Hz, with a ratio between consecutive frequencies of half-octave, and smoothing parameters γ and η equal to 0.5 were used to implement the GF bank.

Mean and standard deviation of the magnitude value of the filtered images were used as texture features [38]. As a result, a feature pattern composed of 48 elements (2 features per filter and a total of 24 filters) was used to describe the texture.

2.4. Local binary patterns

The local binary pattern (LBP) operator was introduced by Ojala et al. [39]. It assumes that texture is composed of different patterns or local spatial structures that are repeated in the image. The LBP seeks to detect them by acting as a template mask that is evaluated at each image pixel. An estimate of the probability of occurrence of these structures is obtained by means of a histogram, which is used to describe the texture.

LBP was defined for gray-scale images. Given a central pixel, it is computed in a neighbourhood of P pixels equally distributed on a circumference of radius R [39]:

$$LBP_{P,R} = \sum_{p=0}^{P-1} s\left(g_p - g_c\right)2^p , \tag{9}$$

where g_c is the gray level of the central pixel and g_p is the gray level of its neighbours. The formulation of $LBP_{P,R}$ yields a total of 2^P different patterns. The probability associated with each of them is estimated by means of its relative frequency, leading to a histogram with 2^P bins. However, for P high enough, a large number of bins is obtained, resulting in sparse histograms. Additionally, although the $LBP_{P,R}$ operator is insensitive to monotonic transformations of the gray scale, it notably changes when the image is rotated.

It was observed that certain local binary patterns are fundamental properties of texture, providing the vast majority of the patterns observed in the texture image [39]. These were called uniform patterns, being characterized for a maximum of two bit transitions in their binary representation. They are identified with structures such as bright spot, flat area or dark spot, and edges. The operator $U(LBP_{P,R})$ was introduced for an accurate definition of uniform patterns. It

accounts for the number of bit transitions in the $LBP_{P,R}$ pattern. From this concept of uniformity, a new rotation-invariant operator $LBP_{P,R}^{riu2}$ was defined:

$$LBP_{P,R}^{riu2} = \begin{cases} \sum_{p=0}^{P-1} s\left(g_p - g_c\right) & \text{if } U\left(LBP_{P,R}\right) \le 2 \\ P+1 & \text{otherwise} \end{cases}, \tag{10}$$

where

$$\begin{aligned} U\left(LBP_{P,R}\right) = &\left|s\left(g_{P-1} - g_c\right) - s\left(g_0 - g_c\right)\right| \\ &+ \sum_{p=1}^{P} \left|s\left(g_p - g_c\right) - s\left(g_{p-1} - g_c\right)\right|. \end{aligned} \tag{11}$$

The operator $LBP_{P,R}^{riu2}$ is capable of identifying P + 2 different patterns, which represents a substantial reduction when compared with the initial $LBP_{P,R}$ operator. As a result, a more reliable estimation of the histogram defining the texture is obtained.

The design of the $LBP_{P,R}^{riu2}$ operator involves defining the values of P and R. They are related to the resolution of the neighbourhood under analysis and its size. Previous experiments evaluated several combinations of these parameters in texture classification [39]. The reported results indicate that P = 24 and R = 3 outperformed other configurations of $LBP_{P,R}^{riu2}$. Thus, these values were used in our experiments. As described, a histogram representing the relative frequency of occurrence for each of the P + 2 structures was used as the texture feature pattern. The number of bins, P + 2, determines the dimension of this pattern.

2.5. Regularized discriminant analysis

The analysis of an image using one of the described methods produces a multivariate feature pattern. It summarizes the information in the texture according to the properties exhibited by the corresponding method. Multivariate pattern analysis is subsequently required to classify the resulting pattern into one of several categories. In this study, supervised classification is proposed using regularized discriminant analysis (RDA) [33].

RDA generalizes the concept of discriminant analysis (DA), including quadratic discriminant analysis (QDA) and linear discriminant analysis (LDA) as special cases. It addresses the problem of covariance matrix estimation in high dimensional spaces. Covariance matrix estimates become highly variable when the number of samples in each category is small compared with the dimension of the input feature space. As a result, the output of the DA classifier may be biased by the smallest eigenvalues [33]. This situation is commonly observed in image processing applications due to the increased dimension of the patterns to be processed. Friedman suggested a method to prevent this problem based on regularization techniques [33]. The idea is to improve the estimates of the covariance matrices by reducing the variance associated with the sample-based estimate while increasing the bias. This adjustment is determined by two parameters λ and μ, which take values between 0 and 1.

The parameter λ controls the choice between QDA ($\lambda = 0$) and LDA ($\lambda = 1$). On the other hand, μ controls the effect of decreasing the larger eigenvalues while increasing the smaller ones. As a result, the bias derived from the sample-based estimation of the covariance matrix is removed [33]. There is no previous knowledge about the most appropriate values of these regularization parameters. Thus, a wide set of combinations of λ and μ were evaluated by

varying them from 0 to 1 with steps of 0.1. The configuration with the highest performance was retained as the optimum.

3. Data and experimental results

Texture images from Brodatz [34], Outex [35] and VisTex [36] databases were employed for a comparative analysis between the proposed DTM-based method and the three conventional techniques used as reference: GLCM, GF and LBP. Different experiments were designed from the selected texture images. A description of the proposed experiments and the achieved results is provided in this section.

3.1. Public databases

3.1.1. Brodatz database

Thirteen textures from the Brodatz album included in the image database of the Signal and Image Processing Institute at the University of Southern California [34] were processed in our experiments: bark (D12), brick (D94), bubbles (D112), grass (D9), leather (D24), pigskin (D92), raffia (D84), sand (D29), straw (D15), water (D38), weave (D16), wood (D68) and wool (D19). The number in parenthesis indicates the page number of the Brodatz texture book where the original image can be found. A set of 7 gray scale images are available for each of these textures depending on their orientation: 0, 30, 60, 90, 120, 150 and 200 degrees. Each of them has a size of 512 x 512 pixels (8 bits per pixel).

3.1.2. Outex database

The Outex database [35] contains 320 colour texture images. Each of them was captured using six spatial resolutions (100, 120, 300, 360, 500 and 600 dpi) and nine rotation angles (0, 5, 10, 15, 30, 45, 60, 75 and 90 degrees). Images are stored in RGB format with a resolution of 24 bits

and a size of 538 x 746 pixels. In our study, 29 textures (the first one in each category) were selected from the Outex database: barleyrice001, canvas001, cardboard001, carpet001, chips001, crushedstone001, flakes001, four001, foam001, fur001, granite001, granular001, gravel001, groats001, leather001, mineral001, paper001, pasta001, pellet001, plastic001, quartz001, rubber001, sand001, sandpaper001, seeds001, tile001, wallpaper001, wood001 and wool001. The luminance channel was extracted to obtain gray scale images with a resolution of 8 bits per pixel. Images with a spatial resolution of 100 dpi and horizon sunlight illumination were selected from the database for our experiments. Nine different images were extracted for each texture by including all the available orientations.

3.1.3. VisTex database

The VisTex database [36] provides a set of texture images that are representative of real-world scenarios. In our study, images labelled as "reference textures" in the VisTex database were considered. These textures are grouped depending on the object represented in the image: bark, grass, water, brick, clouds, etc. They are stored in RGB format with a resolution of 24 bits. In our study, colour information was discarded, converting them to gray scale texture images. A subset of 20 images of size 512 x 512 from this database was evaluated in our experiments: bark0006, brick0000, brick0004, clouds0001, fabric0013, fabric0017, flowers0006, food0000, food0001, grass0001, leaves0012, metal0002, metal0004, misc0001, misc0002, sand0000, sand0002, tile0008, waer0005 and wood0002. It is worth to remark that the same subset was used by other researchers for the evaluation of other texture analysis techniques [8].

3.2. Results

Several experiments were carried out using texture images from Brodatz, Outex and VisTex datasets. A common methodology was adopted for a fair comparison between DTM, GLCM, GF

and LBP. It consists in feature extraction using one of these methods and classification of the resulting feature pattern by means of RDA. In our experiments, the influence of the evaluated dataset, the image size and the orientation of the texture on classification performance was assessed.

3.2.1. Classification of non-rotated textures

The first set of experiments involves textures with a fixed orientation. Brodatz and Outex datasets contain texture samples captured at different angles. Thus, those textures with a rotation of 0 degrees were selected. In the case of the VisTex dataset, all the available textures were included in this set of experiments as they have a unique orientation. As a result, three different datasets were used in the first phase of the experiments: 13 Brodatz textures of size 512 x 512, 29 Outex textures of size 746 x 538 and 20 VisText textures of size 512 x 512. For the three datasets, one texture image was available per each category. The utility of the proposed feature extraction methods was separately evaluated on these datasets. For each of them, four different classification tasks were defined depending on the size of the texture to be processed: 128 x 128, 64 x 64, 32 x 32 and 16 x 16.

The hold-out approach was used to estimate the performance of DTM, GLCM, GF and LBP [24]. Independent training and test sets were generated by dividing the original texture image in each category into two non-overlapping subimages of size 256 x 512, 373 x 538 and 256 x 512 pixels for textures from Brodatz, Outex and VisTex datasets, respectively. One of these subimages was used to extract training samples while the other was allocated for testing. Overlapped texture regions were extracted from each of them to obtain sufficiently large training and test sets. For all the image sizes considered in the experiments, the training set was composed of textures samples defined by a sliding window with an overlapping of 75% on the

training subimage. Overlapping was minimized to obtain images in the test set in order to prevent bias in classification results. Thus, 50% overlapping was used to generate test images of size 128 x 128 and 64 x 64 while 25% and 0% overlapping was used for extracting texture regions of size 32 x 32 and 16 x 16, respectively.

For each classification task, a RDA classifier was implemented form data in the training set. Subsequently, the accuracy achieved on the test set was computed. It was estimated as the ratio between the number of textures correctly classified and the total number of samples. The highest classification accuracy from all the evaluated pairs of parameters λ and μ was retained. Table 1 summarizes the experimental setup and the classification accuracy achieved by the evaluated methods. As can be observed, the most effective method depends on the dataset and the size of the textures. GLCM and GF achieved the highest performance on Brodatz textures while the proposed DTM-based method outperformed the others when images from the Outex dataset were processed. On the other hand, smaller differences are appreciated on VisTex textures. This dataset showed to be the least difficult as DTM, GLCM and GF provided high accuracy on it for all the evaluated texture sizes.

INSERT TABLE 1 AROUND HERE

For all the methods assessed in the study, accuracy decreased as the size of the texture was reduced. This was an expected behaviour as textures are characterized by the repetition of patterns in the spatial domain [1]. Thus, small regions may not capture a sufficient number of these patterns. The decrease in classification performance due to this effect was specially marked for LBP. This is motivated by the estimation of the histogram representing the relative frequency

for each structure identified by the uniform LBP patterns. The number of pattern samples is limited by the dimension N x N of the texture under analysis. As this dimension is reduced, a smaller number of samples is available to compute the histogram, resulting in a poor estimation of the statistical behaviour of these patterns and, thus, of the texture.

The method based on DTM has demonstrated to provide useful information about texture since high classification accuracy was achieved on the proposed problems. An index of separability (*SI*) was computed for each element of $M(s)$ to determine the range of s at which textures show higher differences. This index was obtained as the ratio between the inter-class variability and the intra-class variability [41]. Figure 3 depicts the dependence of *SI* on the moment order s for Brodatz, Outex and VisTex textures. As shown by classification accuracy, the discriminant power decreases as the texture is smaller. In addition, the plot reflects that higher separability between categories relies on the first half of s values in the case of Outex textures while the curve is approximately symmetric for Brodatz and VisTex images. Thus, most of the information representing distinctive texture attributes is contained at intermediate order values.

INSERT FIGURE 3 AROUND HERE

3.2.2. Classification of rotated textures

The robustness of the four feature extraction methods to texture rotation was evaluated in the second set of experiments. These were carried out only from images in Brodatz and Outex datasets since they provide originally rotated textures. The former includes 13 different texture categories. Seven original images are available per category, each of them corresponding to a

different orientation. The latter is composed of 29 texture categories and 9 different orientations per category. As in the previous experiments, textures from both datasets were processed separately.

The original textures were divided into two non-overlapping subimages, which were respectively used to generate training and test samples. As in the previous set of experiments, subimages from the Brodatz dataset have a size of 256 x 512 pixels while those from the Outex dataset are 373 x 538. For the four image sizes assessed in the experiments (i.e., 128 x 128, 64 x 64, 32 x 32 and 16 x 16), training samples were generated using a sliding window with 50% overlapping between adjacent regions. In these experiments, no overlapping was used to extract texture regions for samples in the test set.

Table 2 shows the details of the experiments performed from both Brodatz and Outex rotated textures. As in the previous test, the results show a strong dependence of GLCM on the dataset. Additionally, this second set of experiments reflects that LBP provided the highest classification accuracy when sufficiently large textures (128 x 128) were considered. However, its performance notably decreased as the region size was reduced.

INSERT TABLE 2 AROUND HERE

The comparison between the results on non-rotated and rotated textures reveals that only LBP achieved similar performance in both cases. In contrast, for the other methods, classification accuracy decreased when rotated textures are processed. This result reflects the rotation invariant property of the evaluated LBP operator [39]. However, it is worth noting that, even though this

property is not shared by the other methods, they are also capable of providing reasonable results on rotated textures.

To analyze the robustness of the DTM method against rotation, we evaluated the separability between $M(s)$ curves derived from a given texture image at different rotation angles. Figure 4 shows the *SI* between images from the same texture but with a different rotation: 0, 30, 60, 90, 120, 150 and 200 degrees. For this example, four 32 x 32 Brodatz textures were selected. According to the value of *SI*, differences due to orientation tend to be more appreciable in textures characterized by structures with a marked directional behaviour. This is the case of "Wood" and "Weave" textures. In contrast, for those textures in which structures seem to be repeated along all directions, the $M(s)$ curves corresponding to different orientations are closer to each other, exhibiting higher similarity between them. This behaviour can be found in "Bubbles" and "Sand" textures.

INSERT FIGURE 4 AROUND HERE

4. Discussion and conclusions

A novel method for texture characterization based on DTM was presented. A feature pattern $M(s)$ is derived from the moment matrix. It represents the response of the texture image to the set of filters implemented by the Tchebichef polynomials of order s. To assess the utility of our method, several texture classification problems have been proposed using images from Brodatz, Outex and VisTex datasets. A comparative analysis was performed by evaluating other conventional approaches for texture analysis such as GLCM, GF and LBP on the same

experiments. The results indicate that the proposed $M(s)$ pattern captures essential information about texture, showing its potential for effective texture identification.

Three main conclusions can be drawn from our experiments. First, the method based on DTM represents a valid approach for texture characterization. The performance achieved by our method was comparable to that of GLCM, GF and LBP, which are recognized by the scientific community in the field as effective approaches to texture analysis [1, 5, 39]. Indeed, the proposed DTM-based method achieved the highest average classification accuracy over all the experiments with a value of 85.66% whereas it was 76.90%, 83.29% and 69.81% for GLCM, GF and LBP, respectively. Second, the DTM-based method has shown to be robust since it yielded reasonable results regardless of the dataset or the texture size. It was observed that the performance of other methods highly depended on the image dataset under analysis. Specifically, in the case of GLCM, it provided an average accuracy of 88.12%, 57.32% and 93.62% for experiments involving Brodatz, Outex and VisTex images, respectively. These three average values were 82.64%, 84.72% and 93.59% for the method based on DTM, 84.59%, 78.23% and 90.81% for GF and, 71.78%, 66.75% and 72.03% for LBP. These methods were less influenced by the dataset than GLCM, which markedly failed on Outex textures. On the other hand, for all the evaluated methods, decreasing the size of the texture resulted in reduced performance. However, this reduction was less remarkable for the method based on DTM. For the five classification problems analyzed in this study, the average reduction in the classification accuracy when considering a size $N = 16$ with respect to $N = 128$ was of 27.66%, 33.32%, 38.39% and 69.99% for DTM, GLCM, GF and LBP, respectively. As can be observed, the dependence on the texture size is more pronounced in GLCM and GF than in our DTM-based method while it is dramatic in the case of LBP. Third, satisfactory classification accuracy was

achieved by means of DTM, GLCM and GF on rotated textures even though they are not rotation invariant. For a given image size, the average difference between the accuracy achieved on non-rotated and rotated textures was 2.72, 7.34 and 6.46 percentage points for DTM, GLCM and GF, respectively. These data were computed by comparing the results achieved on non-rotated and rotated textures from Brodatz and Outex datasets. DTM, GLCM and GF reflected a higher dependence on this effect than LBP. The latter showed similar performance on both non-rotated and rotated textures (the average difference was 0.99 percentage points) since it is the only method that is invariant to rotation. However, for most of the textures, there is not a clear orientation of the structures characterizing them. Therefore, rotation does not have a marked effect on their attributes. This suggests that the feature patterns extracted from rotated versions of the same image using DTM, GLCM and GF tend to be similar. In the case of DTM, this was observed by analyzing the influence of rotation on the $M(s)$ curve. It was concluded that higher variability between curves from the same texture at different rotation angles is found when the texture is characterized by structures with a dominant orientation.

Previous techniques for texture characterization based on DTM, or on the closely related DCT, substantially differ from the methodology described in the present study. Indeed, only low order moments were considered as texture features [29, 30]. Nevertheless, according to our results, a more accurate description of texture properties can be obtained by analyzing the whole range of moment orders. The full set of DTM is required for exact image reconstruction and, thus, it is worthwhile to consider each moment for the complete description of texture. Moments of increased order capture higher frequency components characterizing the texture. Therefore, these moments contain valuable information in the case of textures distinguished by rapidly varying patterns. The relevance of the moment order in a given classification task was quantified

by the *SI*, which reflected that some degree of discriminant capability is provided by each element of the $M(s)$ pattern. In particular, higher values of this index were found for intermediate values of s, proving that moments with a certain order may be essential for texture identification.

In our method, $M(s)$ was defined by only considering the magnitude of the moments, discarding the sign information. However, the sign of DTM may provide useful knowledge about the image. A connection between the sign of the DCT coefficients and the phase of the Fourier transform has been suggested elsewhere [42]. Indeed, image retrieval based on the sign of DCT coefficients has yielded promising results [43]. On the other hand, phase information plays a relevant role in applications involving texture analysis such as iris recognition [4]. As a result, further analysis on the utility of the sign of DTM is required.

Several limitations can be found in our methodology. As indicated, the proposed $M(s)$ signature provides a compact global representation of texture properties. Nevertheless, the dimension of the resulting pattern ($2N - 1$) may be too large for adequate statistical modelling. For high values of N, overfitting may arise when using complex classifiers such as neural networks [24]. To prevent this effect, we suggest summarizing the information in the $M(s)$ curve by defining a reduced set of descriptors. For a given texture classification problem, it would be required to identify those descriptors that provide high discrimination ability between texture categories. Furthermore, this approach can also be considered in order to combine DTM features with those derived from other procedures. On the other hand, our method is not invariant to image transformations. Although it achieved reasonable performance on rotated textures, invariant properties must be addressed in further development of the method. They are a crucial issue in order to deal with a wider variety of pattern recognition problems. In this context, radial

Tchebichef moments were proposed to obtain rotation invariant descriptors from images [44]. Additionally, translation and scale invariants from DTM have been defined [45].

In summary, a method for texture characterization based on DTM was proposed. An exhaustive validation process was carried out by comparing its performance in several texture classification problems with other standard methods used for texture analysis. From our experiments, it was demonstrated that the DTM-based method captures essential information about texture, showing comparable or even higher performance than conventional procedures. Additionally, it is worth noting that the proposed $M(s)$ pattern can be efficiently obtained through computational strategies developed for DTM [21]. Therefore, we conclude that our method can be considered as an efficient tool to be used in image processing problems involving texture classification.

Acknowledgments

J. Victor Marcos is a "Juan de la Cierva" research fellow, funded by the Spanish Ministry of Economy and Competitiveness.

References

1. M. Tuceryan and A.K. Jain, "Texture Analysis," in *The handbook of pattern recognition and computer Vision*, C.H. Chen, L.F. Pau, and P.S.P. Wang, eds. (World Scientific, 1993), 235–276.
2. V.S. Bharathi and L. Ganesan, "Orthogonal moments based texture analysis of CT liver images," Pattern Recognit. Lett. 29, 1868-1872 (2008).
3. L.K. Soh and C. Tsatsoulis, "Texture analysis of SAR sea ice imagery using gray level co-occurrence matrices," IEEE Trans. Geosci. Remote Sensing 37, 780-795 (1999).

4. J. Daugman, “How iris recognition works,” IEEE Trans. Circuits Syst. Video Technol. 14, 21-30 (2004).
5. T. Randen and J.H. Husoy, “Filtering for texture classification: a comparative study,” IEEE Trans. Pattern Anal. Mach. Intell. 21, 291-310 (1999).
6. J. Beck, A. Sutter, and R. Ivry, “Spatial frequency channels and perceptual grouping in texture segregation,” Comput. Gr. Image Process. 37, 299-325 (1987).
7. X. Liu and D. Wang, “Texture classification using spectral histograms,” IEEE Trans. Image Process. 12, 661-670 (2003).
8. S. Arivazhagan and L. Ganesan, “Texture classification using wavelet transform,” Pattern Recognit. Lett. 24, 1513-1521 (2003).
9. A.K. Jain and F. Farrokhnia, “Unsupervised texture segmentation using Gabor filters,” Pattern Recognit. 24, 1167-1186 (1991).
10. G.M. Haley and B.S. Manjunath, “Rotation-invariant texture classification using a complete space-frequency model,” IEEE Trans. Image Process. 8, 255-269 (1999).
11. M.K. Hu, “Visual pattern recognition by moment invariants,” IEEE Trans. Inf. Theory 8, 179-187 (1962).
12. J. Flusser, T. Suk, and B. Zitová, *Moments and moment invariants in pattern recognition* (John Wiley & Sons, 2009).
13. J. Bigun and J.M. Hans du Buf, “N-folded symmetries by complex moments in Gabor space and their application to unsupervised texture segmentation,” IEEE Trans. Pattern Anal. Mach. Intell. 16, 80-87 (1994).
14. M. Wang and A. Knoesen, “Rotation- and scale-invariant texture features based on spectral moment invariants,” J. Opt. Soc. Am. A 24, 2550-2557 (2007).

15. R. Mukundan, S.H. Ong, and P.A. Lee, “Image analysis by Tchebichef moments,” IEEE Trans. Image Process. 10, 1357-1364 (2001).
16. S.X. Liao and M. Pawlak, “On image analysis by moments,” IEEE Trans. Pattern Anal. Mach. Intell. 18, 254-266 (1996).
17. M.R. Teague, “Image analysis via the general theory of moments,” J. Opt. Soc. Am. A 70, 920-930 (1980).
18. C.H. Teh and R.T. Chin, “On image analysis by the methods of moments,” IEEE Trans. Pattern Anal. Mach. Intell. 10, 496-513 (1988).
19. B. Bayraktar, T. Bernas, J.P. Robinson, and B. Rajwa, “A numerical recipe for accurate image reconstruction from discrete orthogonal moments,” Pattern Recognit. 40, 659-669 (2007).
20. P.T. Yap, R. Paramesran, and S.H. Ong, “Image analysis by Krawtchouk moments,” IEEE Trans. Image Process. 12, 1367-1377 (2003).
21. R. Mukundan, “Some computational aspects of discrete orthonormal moments,” IEEE Trans. Image Process. 13, 1055-1059 (2004).
22. C.Y. Wee, R. Paramesran, R. Mukundan, and X. Jiang, “Image quality assessment by discrete orthogonal moments,” Pattern Recognit. 43, 4055-4068 (2010).
23. P.T. Yap and P. Raveendran, “Image focus measure based on Chebyshev moments,” IEE Proceedings on Vision, Image and Signal Processing 151, 128-136 (2004).
24. C.M. Bishop, *Neural networks for pattern recognition* (Oxford Univesity Press, 1995).
25. K.H. Thung, R. Paramesan, and C.L. Lim, “Content-based image quality metric using similarity measure of moment vectors,” Pattern Recognit. 45, 2193-2204 (2012).

26. C. Deng, X. Gao, X. Li, and D. Tao, "A local Tchebichef moments-based robust image watermarking," Signal Process. 89, 1531-1539 (2009).
27. H. Huang, G. Coatrieux, H.Z. Shu, L.M. Luo, and C.R. Roux, "Blind forensics in medical imaging based on Tchebichef image moments," in Proceedings of the 33rd Annual International Conference of the IEEE-EMBS (IEEE, 2011), 4473-4476.
28. K. Nakagaki and R. Mukundan, "A fast 4 x 4 forward discrete Tchebichef transform algorithm," IEEE Signal Process. Lett. 14, 684-687 (2007).
29. B. Li and M.Q.H. Meng, "Computer-aided detection of bleeding regions for capsule endoscopy images," IEEE Trans. Biomed. Eng. 56, 1032-1039 (2009).
30. K. Wu, C. Garnier, J.L. Coatrieux, and H. Shu, "A preliminary study of moment-based texture analysis for medical images," in Proceedings of the 32nd Annual International Conference of the IEEE-EMBS (IEEE, 2010), 5581-5584.
31. K.W. See, K.S. Loke, P.A. Lee, and K.F. Loe, "Image reconstruction using various discrete orthogonal polynomials in comparison with DCT," Appl. Math. Comput. 193, 346-359 (2007).
32. D.G. Sim, H.K. Kim, and R.H. Park, "Fast texture description and retrieval of DCT-based compressed images," Electron. Lett. 37, 18-19 (2001).
33. J.H. Friedman, "Regularized discriminant analysis," J. Am. Stat. Assoc. 84, 165-175 (1989).
34. A.G. Weber, "The ISC-SIPI image database," University of Southern California, (Technical Report, 1997).
35. T. Ojala, T. Mäenpää, M. Pietikäinen, J. Viertola, J. Kyllönen, and S. Huovinen, "Outex – New framework for empirical evaluation of texture analysis algorithms," in Proceedings of the 16th International Conference on Pattern Recognition (IEEE, 2002), 701-706.

36. MIT Media Laboratory, "VisTex Vision Texture Database," http://vismod.media.mit.edu/vismod/imagery/VisionTexture/
37. R.M. Haralick, K. Shanmugam, and I. Dinstein, "Textural features for image classification," IEEE Trans. Syst. Man Cybern. SMC-3, 610-621 (1973).
38. F. Bianconi and A. Fernández, "Evaluation of the effects of Gabor filter parameters on texture classification," Pattern Recognition 40, 3325-3335 (2007).
39. T. Ojala, M. Pietikäinen, and T. Mäenpää, "Multiresolution gray-sclae and rotation invariant texture classification with local binary patterns," IEEE Trans. Pattern Anal. Mach. Intell. 24, 971-987 (2002).
40. J.G. Daugman, "Two-dimensional spectral analysis of cortical receptive fields profile," Vision Res. 20, 847-856 (1980).
41. P. Gallinari, S. Thiria, F. Badran, and F. Fogelman-Soulie, "On the relations between discriminant analysis and multilayer perceptrons," Neural Netw. 4, 349-360 (1991).
42. Ito and H. Kiya, "DCT sign-only correlation with application to image matching and the relationship with phase-only correlation," in Proceedings of the IEEE International Conference on Acoustics, Speech and Signal Processing 2007 (IEEE, 2007), I1237-I1240.
43. F. Arnia, I. Iizuka, M. Fujiyoshi, and H. Kiya, "Fast image identification methods for JPEG images with different compression ratios," IEICE Trans. Fundam. Electron. Commun. Comput. Sci. E89-A, 1585-1593 (2006).
44. R. Mukundan, "A new class of rotational invariants using discrete orthogonal moments," in Proceedings of the 6th IASTED International Conference on Signal and Image Processing (IASTED, 2004), 80-84.

45. H. Zhu, H. Shu, T. Xia, L. Luo, and J.L. Coatrieux, “Translation and scale invariants of Tchebichef moments,” Pattern Recognit. 40, 2530-2542 (2007).

Figures

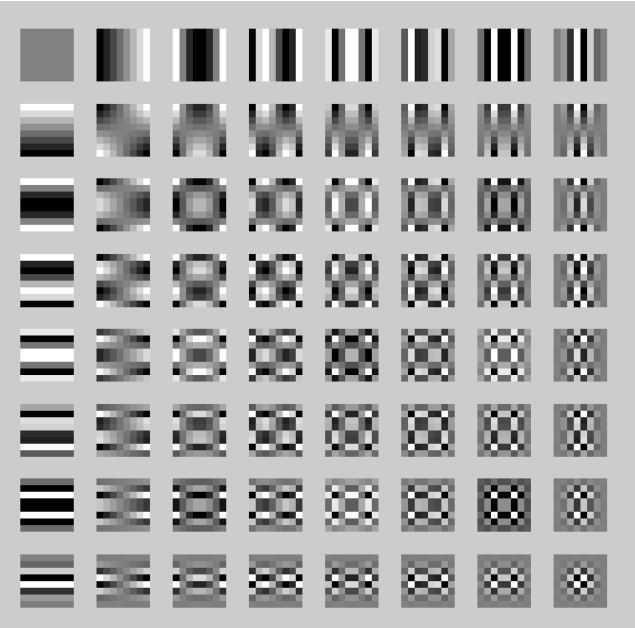

Fig. 1. Complete set of Tchebichef kernels for $N = 8$.

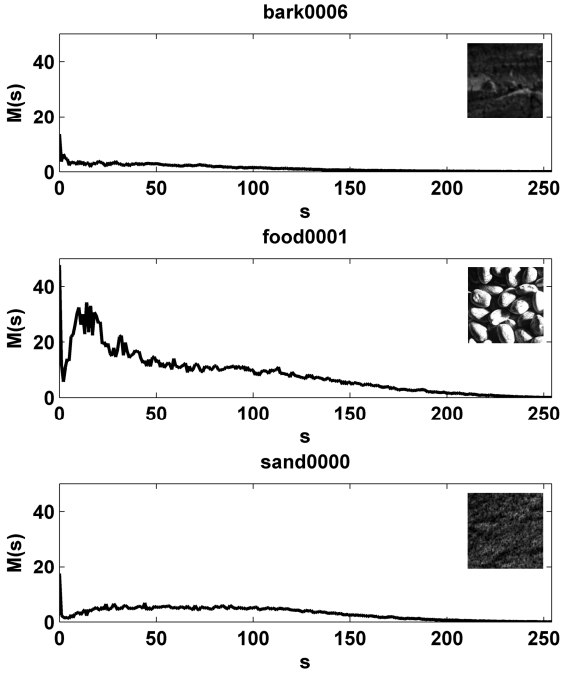

Fig. 2. $M(s)$ curves corresponding to three textures of size 128 x 128 from the VisTex database.

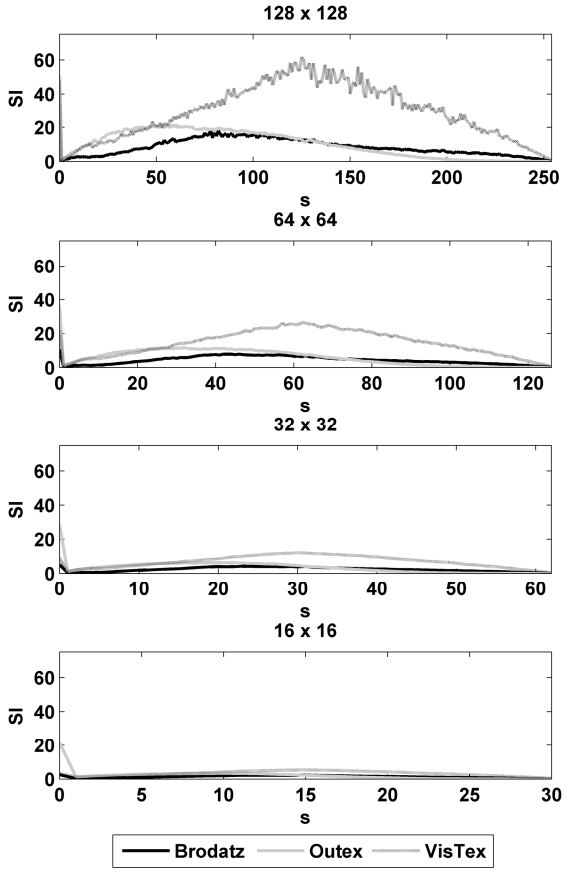

Fig. 3. Evolution of the *SI* of coefficients $M(s)$ as a function of the moment order for Brodatz, Outex and VisTex datasets.

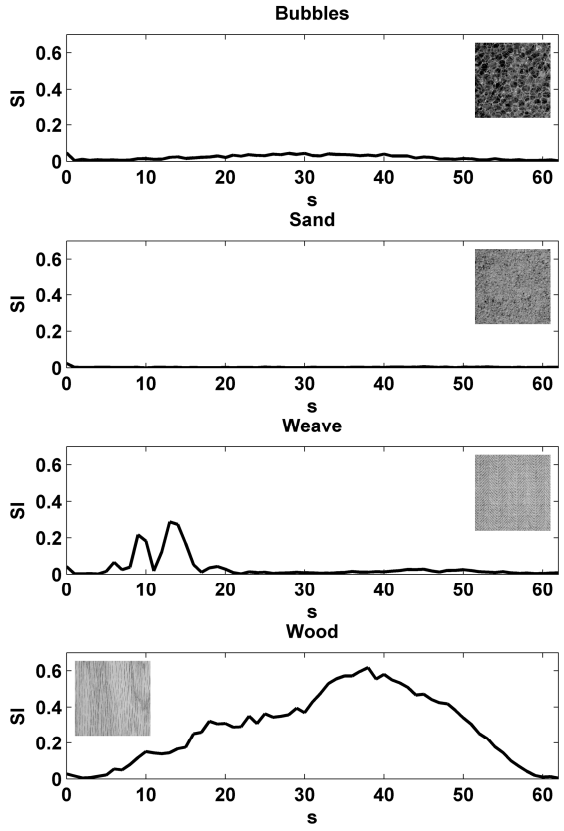

Fig. 4. Evolution of the *SI* between $M(s)$ curves from the same texture captured at different orientation angles. Results computed from four textures in the Brodatz dataset.

Tables

Table 1. Classification of non-rotated textures[a]								
Dataset	Brodatz							
N_{cat}	13							
N_{ipc}	1 (512 x 512)							
Size	128 x 128		64 x 64		32 x 32		16 x 16	
Set	Train	Test	Train	Test	Train	Test	Train	Test
Ovp	75	50	75	50	75	25	75	0
N_{samp}	65	21	377	105	1769	210	7625	512
DTM	99.27		89.74		80.84		66.87	
GLCM	**100**		98.61		**91.14**		**73.02**	
GF	**100**		**98.68**		89.56		67.08	
LBP	98.17		89.96		63.77		32.89	
Dataset	Outex							
N_{cat}	29							
N_{ipc}	1 (538 x 746)							
Size	128 x 128		64 x 64		32 x 32		16 x 16	
Set	Train	Test	Train	Test	Train	Test	Train	Test
Ovp	75	50	75	50	75	25	75	0
N_{samp}	104	28	600	150	2752	330	11790	759
DTM	94.46		90.83		**84.68**		**72.50**	
GLCM	78.33		69.33		56.50		44.17	
GF	93.72		**91.13**		80.18		56.79	
LBP	**95.44**		87.70		59.40		26.07	
Dataset	VisTex							
N_{cat}	20							
N_{ipc}	1 (512 x 512)							
Size	128 x 128		64 x 64		32 x 32		16 x 16	
Set	Train	Test	Train	Test	Train	Test	Train	Test
Ovp	75	50	75	50	75	25	75	0
N_{samp}	65	21	377	105	1769	210	7625	512
DTM	**100**		**99.00**		95.19		80.17	
GLCM	99.76		97.62		**95.29**		**81.82**	
GF	98.81		97.57		93.48		73.37	
LBP	98.57		93.14		66.52		29.87	

[a] N_{cat}: number of distinct categories in the classification problem; N_{ipc}: number of available images per category; Ovp: overlapping percentage between adjacent samples; N_{samp}: number of samples.

Table 2. Classification of rotated textures[a]								
Dataset	Brodatz							
N_{cat}	13							
N_{ipc}	7 (512 x 512)							
Size	128 x 128		64 x 64		32 x 32		16 x 16	
Set	Train	Test	Train	Test	Train	Test	Train	Test
Ovp	50	0	50	0	50	0	50	0
N_{samp}	147	56	735	224	3255	896	13671	3584
DTM	96.29		90.01		77.34		60.79	
GLCM	97.66		**94.81**		**84.58**		**65.12**	
GF	98.90		92.58		77.66		52.28	
LBP	**99.59**		92.48		64.43		32.91	
Dataset	Outex							
N_{cat}	29							
N_{ipc}	9 (538 x 746)							
Size	128 x 128		64 x 64		32 x 32		16 x 16	
Set	Train	Test	Train	Test	Train	Test	Train	Test
Ovp	50	0	50	0	50	0	50	0
N_{samp}	252	72	1350	360	6336	1584	26730	6831
DTM	91.57		**91.72**		**83.96**		**68.04**	
GLCM	66.95		57.87		48.39		37.01	
GF	92.96		88.11		73.43		49.53	
LBP	**95.45**		86.63		58.57		24.70	

[a] N_{cat}: number of distinct categories in the classification problem; N_{ipc}: number of available images per category; Ovp: overlapping percentage between adjacent samples; N_{samp}: number of samples.